4724 *Chem. Mater.* **2009,** *21,* 4724–4730
DOI:10.1021/cm902050j

CHEMISTRY OF MATERIALS
Article

Hierarchically Structured Sulfur/Carbon Nanocomposite Material for High-Energy Lithium Battery

Chengdu Liang,*,† Nancy J. Dudney,‡ and Jane Y. Howe‡

†*Center for Nanophase Materials Sciences and* ‡*Materials Science and Technology Division, Oak Ridge National Laboratory, Oak Ridge, Tennessee 37831*

Received July 7, 2009. Revised Manuscript Received August 22, 2009

We report herein a hierarchically structured sulfur−carbon (S/C) nanocomposite material as the high surface-area cathode for rechargeable lithium batteries. A porous carbon with a uniform distribution of mesopores of 7.3 nm has been synthesized through a soft-template synthesis method. The potassium hydroxide activation of this mesoporous carbon results in a bimodal porous carbon with added microporosity of less than 2 nm to the existing mesopores without deterioration of the integrity of the original mesoporous carbon. Elemental sulfur has been loaded to the micropores through a solution infiltration method. The resulted S/C composites with various loading level of sulfur have a high surface areas and large internal porosities. These materials have been tested as novel cathodes for Li/S batteries. The results show that the cyclability and the utilization of sulfur in the Li/S batteries have been significantly improved. The large internal porosity and surface area of the micromesoporous carbon is essential for the high utilization of sulfur.

1. Introduction

With the increasing demand of the world energy consumption, electrical energy storage is recognized as an essential element for both stationary and mobile power sources. Li-ion batteries have been widely used as the primary electrical energy storage devices in various portable electronics because of their lightweight relative to other types of batteries. However, for large applications such as electrical vehicles (EVs), the current Li-ion battery technology does not meet the high energy and high power requirements. The major obstacle lies in the fundamental cathode chemistry, which uses transition metal compounds to store electrical energy: the heavy transition metals put a theoretical limit to the current Li-ion batteries and make the goal of driving EVs on Li-ion batteries hard to reach. Lithium−sulfur chemistry, though less studied, holds great promise for achieving the goal of EV battery applications based on the sulfur chemistry, which has a theoretical capacity of 1675 mA h g^{-1}, nearly one magnitude higher than that of $LiFePO_4$ (theoretical capacity 176 mA h g^{-1}), a material current studied for high power hybrid electrical vehicles (HEVs). Nevertheless, the Li/S system has not been implemented in EVs because of two fatal hurdles: the poor electrical conductivity of elemental sulfur and the intrinsic polysulfide shuttle.

The electrical conductivity of elemental sulfur is as low as 5×10^{-30} S/cm at 25 °C.[1,2] Such a low conductivity causes poor electrochemical contact of the sulfur and leads to low utilization of active materials in the cathode. Although compositing elemental sulfur with carbon or conducting polymers significantly improves the electrical conductivity of sulfur containing cathodes,[3−5] the porous structure of the cathode still needs optimization to facilitate the transport of ions while retaining a good integrity of the cathode after the dissolution of sulfur at the discharge cycle.

The sulfur in the cathode, except at the full charge state, is present as a solution of polysulfides in the electrolyte.[6] The concentration of polysulfide species S_n^{2-} with n greater than 4 at the cathode is always higher than that at the anode; and the concentration of S_n^{2-} with n smaller than 4 is higher at the anode than the cathode. The concentration gradients of the polysulfide species drive the intrinsic polysulfide shuttle between the electrodes, and lead to poor cyclability, high current leakage, and low charge/discharge efficiency.[6] A portion of the polysulfide is transformed into lithium sulfide and deposited on the anode. This deposition process occurs in every charge/discharge cycle and eventually leads to the complete loss of capacity of the sulfur cathode. The deposition of lithium sulfide also leads to an increase of internal cell resistance because of the insulating nature of lithium sulfide. Progressive increases in charging voltage and

*Corresponding author. E-mail: liangcn@ornl.gov.

(1) Dean, J. A. *Lange's Handbook of Chemistry*, 3rd ed.; McGraw-Hill Professional: New York, 1985.
(2) Wang, J.; Chew, S. Y.; Zhao, Z. W.; Ashraf, S.; Wexler, D.; Chen, J.; Ng, S. H.; Chou, S. L.; Liu, H. K. *Carbon* **2008**, *46*, 229–235.
(3) Ji, X. L.; Lee, K. T.; Nazar, L. F. *Nat. Mater.* **2009**, *8*, 500–506.
(4) Wang, J.; Chen, J.; Konstantinov, K.; Zhao, L.; Ng, S. H.; Wang, G. X.; Guo, Z. P.; Liu, H. K. *Electrochim. Acta* **2006**, *51*, 4634–4638.
(5) Wang, J. L.; Yang, J.; Wan, C. R.; Du, K.; Xie, J. Y.; Xu, N. X. *Adv. Funct. Mater.* **2003**, *13*, 487–492.
(6) Mikhaylik, Y. V.; Akridge, J. R. *J. Electrochem. Soc.* **2004**, *151*, A1969–A1976.

Published on Web 09/04/2009

decreases in discharge voltage are always observed in Li/S batteries because of the increase of cell resistance in consecutive cycles. Hence, the energy efficiency decreases with the increase of cycle numbers. Enormous amounts of research have been conducted to mitigate the negative effect of the polysulfide shuttle. Much of this research has focused on either the protection of the lithium anode[7] or the restraining of the ionic mobility of the polysulfide anions.[8,9] The protection of the lithium anode leads to the passivation of the anode which causes a slow reaction rate at the anode during the discharge cycle; hence, the protection of the lithium anode leads to the loss of power density. Gel electrolytes and solid electrolytes have been reported as means for slowing down the polysulfide shuttle by reducing the ionic mobility of electrolytes.[8−15] The slow transport of ions also leads to low power density. Nanostructured composite materials, which retain the polysulfides at the cathode region through high surface-area adsorbents, are promising cathode materials for long cycle-life Li/S batteries. However, the use of porous silica,[8] alumina,[16] and mixed metal oxides[17] leads to a low electrical conductivity of the cathode, which is unfavorable of hig-performance electrodes. In this sense, high-surface-area carbon nanotubes and nanofibers are better materials for the sulfur cathodes than the high-surface-area oxides.[15,18−20] Recent reports suggest that porous carbons are the most promising materials for the sulfur cathodes:[3] the cathode made of sulfur on mesoporous carbon shows an excellent rate performance while retaining good cyclability of the cathode at low sulfur loading, however, results in a low energy density;[2] the cathode made of sulfur on microporous carbon shows an excellent cyclability but compromises the rate performance.[21]

We report herein nanostructured sulfur−carbon composite cathodes that can significantly improve the cyclability of Li/S batteries and promote the utilization of sulfur in the battery cycles. The starting material is mesoporous carbon with a rigid framework that was synthesized through a soft-template synthesis method reported by Liang etc.[22−25] The mesoporous carbon is an electrically conductive material with a low electrical resistivity of 4 Ω cm.[26] A bimodal meso/microporous carbon has been synthesized as a high-surface-area cathode material for Li/S batteries. The idea is illustrated in Scheme 1. In brief, uniform mesoporous carbon was activated using potassium hydroxide (KOH); the activated mesoporous carbon has a hierarchical structure with a bimodal pore size distribution of micropores (< 2 nm) and mesopores (7.3 nm). The micropores are presented as intrawall porosity of the mesoporous frameworks. These two sets of pores were utilized to carry out two functions: (1) the micropores were used as microcontainers for elemental sulfur; the high surface area of the micropores provides sufficient contact to the insulating sulfur and conveys a high electrical conductivity to the composite material; and (2) the mesopores facilitate the transport of Li ions during the electrochemical cycling and accommodate the polysulfides and sulfide ions resulting from the electrochemical reactions. The large internal porosity and surface area of the meso/microporous carbon is essential for achieving the high utiltization of sulfur.

Scheme 1. Illustration of the S/C Composite Cathode Material by Using a Bimodal Porous Carbon As the Support

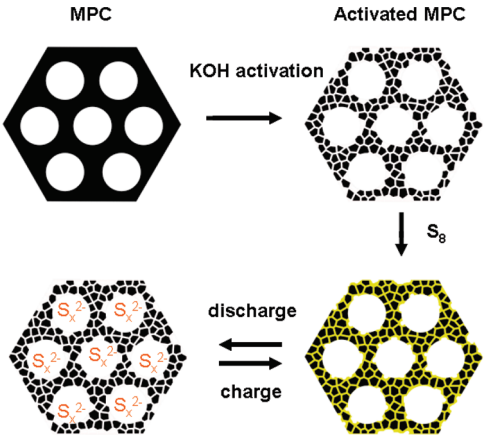

2. Experimental Section

Synthesis of Mesoporous Carbon. The mesoporous carbon (MPC) was synthesized through a soft-template approach reported by Liang et al. with a minor modification.[22−24] In brief, a 2:1 mixture of Pluronic surfactant F127 and phloroglucinol (3.78 g) and hydrochloric acid 37 wt % aqueous solution (0.5 g) were dissolved in 65 mL of absolute ethanol. The solution was then heated to 80 °C with vigorous stirring. An aqueous solution of formaldehyde 37 wt. % (1.3 g) was added to the solution to

(7) Lee, Y. M.; Choi, N. S.; Park, J. H.; Park, J. K. *J. Power Sources* **2003**, *119*, 964–972.
(8) He, X. M.; Shi, Q.; Zhou, X.; Wan, C. R.; Jiang, C. Y. *Electrochim. Acta* **2005**, *51*, 1069–1075.
(9) Wang, J. L.; Yang, J.; Xie, J. Y.; Xu, N. X.; Li, Y. *Electrochem. Commun.* **2002**, *4*, 499–502.
(10) Ryu, H. S.; Ahn, H. J.; Kim, K. W.; Ahn, J. H.; Cho, K. K.; Nam, T. H. *Electrochim. Acta* **2006**, *52*, 1563–1566.
(11) Ryu, H. S.; Ahn, H. J.; Kim, K. W.; Ahn, J. H.; Lee, J. Y. *J. Power Sources* **2006**, *153*, 360–364.
(12) Jeon, B. H.; Yeon, J. H.; Chung, I. J. *J. Mater. Process. Technol.* **2003**, *143*, 93–97.
(13) Shin, J. H.; Jung, S. S.; Kim, K. W.; Ahn, H. J.; Ahn, J. H. *J. Mater. Sci.: Mater. Electron.* **2002**, *13*, 727–733.
(14) Jeong, S. S.; Lim, Y. T.; Jung, B. S.; Kim, K. W. *Mater. Sci. Forum* **2005**, *486−487*, 594–597.
(15) Shim, J.; Striebel, K. A.; Cairns, E. J. *J. Electrochem. Soc.* **2002**, *149*, A1321–A1325.
(16) Choi, Y. J.; Jung, B. S.; Lee, D. J.; Jeong, J. H.; Kim, K. W.; Ahn, H. J.; Cho, K. K.; Gu, H. B. *Phys. Scr.* **2007**, *T129*, 62–65.
(17) Zhang, Y.; Wu, X. B.; Feng, H.; Wang, L. Z.; Zhang, A. Q.; Xia, T. C.; Dong, H. C. *Int. J. Hydrogen Energy* **2009**, *34*, 1556–1559.
(18) Choi, Y. J.; Jeong, S. S.; Kim, K. W.; Ahn, H. J.; Ahn, J. H. *Mater. Sci. Forum* **2006**, *510−511*, 1082–1085.
(19) Jeong, S. S.; Choi, Y. J.; Kim, K. W. *Mater. Sci. Forum* **2006**, *510−511*, 1106–1109.
(20) Kim, J. H.; Choi, Y. J.; Jeong, S. S.; Cho, K. K.; Kim, K. W. *Mater. Sci. Forum* **2005**, *486−487*, 598–601.
(21) Lai, C.; Gao, X. P.; Zhang, B.; Yan, T. Y.; Zhou, Z. *J. Phys. Chem. C* **2009**, *113*, 4712–4716.
(22) Wang, X. Q.; Liang, C. D.; Dai, S. *Langmuir* **2008**, *24*, 7500–7505.
(23) Liang, C. D.; Dai, S. *J. Am. Chem. Soc.* **2006**, *128*, 5316–5317.
(24) Liang, C. D.; Hong, K. L.; Guiochon, G. A.; Mays, J. W.; Dai, S. *Angew. Chem, Int. Ed.* **2004**, *43*, 5785–5789.
(25) Steinhart, M.; Liang, C. D.; Lynn, G. W.; Gosele, U.; Dai, S. *Chem. Mater.* **2007**, *19*, 2383–2385.
(26) Shanahan, P. V.; Xu, L. B.; Liang, C. D.; Waje, M.; Dai, S.; Yan, Y. S. *J. Power Sources* **2008**, *185*, 423–427.

initiate the polymerization reaction. The heating and stirring of the reaction mixture were continued for two hours to ensure completion of the reaction. The resulting orange colored particles were collected through filtration and washed twice with 5 mL of ethanol each. The particles were dried for 2 h in an oven at 140 °C. The carbonization was carried out in N_2 in a tube furnace (Thermolyne, model: 79300) ramping from room temperature to 850 at 2 °C/min. The final temperature was held for 2 h to ensure complete decomposition of the surfactant and carbonization of the phloroglucinol/formaldehyde copolymer.

KOH Activation. The MPC particles (1 g) were mixed with KOH pellets (4 g) in a nickel crucible with a nickel lid. The crucible was heated to 800 °C at a ramp of 10 °C/min in a tube furnace in N_2. The temperature was kept at 800 °C for 1 h and then was cooled to room temperature (***Caution!*** *Hazardous deposition of potassium metal on the ends of the tube furnace may cause it to catch fire when open to air*). The residue in the crucible was washed with copious deionized water and then boiled in 0.1 M HCl for 30 min. The particles were recovered after filtration and washed to neutral with deionized water. The final product of activated mesoporous carbon (a-MPC) was dehydrated at 200 °C for 24 h.

Preparation of S/C Composites. A 10 wt % solution of sulfur in carbon disulfide (CS_2) was prepared by a two step procedure: first, the sulfur was heated to 140 °C and then rapidly cooled down to room temperature with a cold water bath or an air flow; and second, the calculated amount of CS_2 was added to the sulfur while stirring. The solution was filtered with a syringe filter before use. Elemental sulfur was loaded to a-MPC through liquid phase infiltration by using a freshly made solution of 10 wt % sulfur in CS_2. The infiltration of sulfur in a-MPC was carried out through a repetitive solution impregnation/drying procedure to attain samples with various loadings. The carbon disulfide solvent was evaporated in a well-vented hood. After each impregnation/drying cycle, each sample was annealed at 140 °C for 1 h with protection of nitrogen gas. The annealing step stripped away the residual CS_2.

Nitrogen Sorption. A Micromeritic Gemini 275 system was used to measure the nitrogen adsorption isotherms of the porous carbons and the S/C composites. The specific surface areas (SA) and pore size distributions (PSD) were calculated by using the Brunauer−Emmett−Teller (BET) theory and the Barrett−Joyner−Halenda (BJH) method based on the adsorption branches of the isotherms. The specific pore volumes (PV) were measured at relative pressure 0.95.

Thermogravimetric Analysis (TGA). The weight percentages of the S in the S/C composites were measured by TGA on a TA Q-500 TGA system (TA Instruments). The samples were loaded onto platinum sample pans and heated to 500 at 10 °C/min under a nitrogen stream of 50 SCCM.

High-Resolution Scanning Electron Microscopy (HRSEM). HRSEM images were taken on a field emission STEM (Hitachi HF-3300). The pulverized samples were directly loaded to the TEM grids without any additional sample preparation. The TEM was operated at 300 kV.

Preparation of Cathode. The S/C composites were pulverized using a ball mill and sieved through a 25 μm opening stainless steel sieve. Slurries were prepared using the S/C composites and a solution of 1 wt % poly(vinylidene fluoride) (PVDF) in anhydrous *N*-methyl-2-pyrolidinone (NMP) with a ratio of 1:5. The slurries were applied to 10 mm diameter aluminum current collectors and dried at 120 °C for 4 h. For the purpose of comparison, the original mesoporous carbon (MPC) with 24.1 wt % sulfur loading and WVA-1500 (MeadWestvaco Corporation) with sulfur loading of 25.2 wt % were also prepared as cathodes by applying an identical procedure that was used for the preparation of S/C composite cathodes.

Electrochemical Evaluation. The batteries were assembled as Swagelok cells by using the S/C composite coated aluminum foil (10 mm diameter, 7 mm thickness) as the cathode, and a lithium foil (7 mm thickness and 10 mm diameter) as the anode, a Celgard 3225 separator (10.3 mm diameter), and an organic electrolyte. The organic electrolytes were solutions of Bis-(trifluoromethane)sulfonimide lithium (LiTFSI) (99.95% trace metals basis) in a mixed solvent of 1,3-dioxolane (DOL) and dimethoxyethane (DME) with volume ratio of 55:40. The organic electrolyte filled the pores of the cathode and separator. The cathode, separator, and anode were pressed by a spring to ensure tight contact. A typical cell contained about 0.2 mg of sulfur. No excess of electrolyte was left in the assembled cell. The batteries were tested in a Maccor 4000 series battery tester. The batteries were cycled between 1.0 to 3.6 V. Each cycle was started with the discharge half-cycle. Unless specified, all batteries were tested at the same current of 0.5 mA for both charging and discharging. An average current density of 2.5 A/g was used for all cells. The cutoff current for the charge cycle was set to 0.05 mA. The calculation of specific discharge capacities is based on the mass of elemental sulfur.

3. Results and Discussion

3.1. Synthesis of Carbon Materials. The mesoporous carbon (MPC) was synthesized through a soft-template approach reported by Liang et al.[22−24] The MPC has a uniform mesopore distribution at ca. 7.3 nm, an average wall thickness of about 6 nm, a specific Brunauer−Emmett−Teller (BET) surface area of 368.5 m^2/g, and a pore volume of 0.56 cm^3/g. After the KOH activation, the BET surface area of the activated MPC (a-MPC) increased to 1566.1 m^2/g; the micropore surface area contribution is 962.4 m^2/g. The MPC and a-MPC have type IV isotherms with H1 hysteresis (Figure 1a). The pore size distribution plot in Figure 1b shows that there is a significant increase of small mesopores from 2 to 4 nm, while the large mesopores are slight enlarged. The micropore volume of the a-MPC calculated from the thickness-plot (also known as T-plot) is about 0.503 cm^3/g. The characteristics of the a-MPC agree with the reported data of KOH activated mesoporous carbons synthesized through different approaches.[27,28] No morphological changes were observed in the mesoporous carbon following KOH activation based on HRSEM images (not shown in this paper). This observation confirms that the mesoporous carbon synthesized through the soft-template synthesis possesses a rigid framework, which survives harsh chemical treatments.[29]

3.2. Characterization of S/C Nanocomposites. *3.2.1. TGA Analysis.* Elemental sulfur was loaded into a-MPC through liquid phase infiltration by using sulfur solution in carbon disulfide (CS_2). The infiltration of sulfur in a-MPC was carried out through a repetitive solution

(27) Gorka, J.; Zawislak, A.; Choma, J.; Jaroniec, M. *Carbon* **2008**, *46*, 1159–1161.
(28) Choi, M.; Ryoo, R. *J. Mater. Chem.* **2007**, *17*, 4204–4209.
(29) Liang, C. D.; Xie, H.; Schwartz, V.; Howe, J.; Dai, S.; Overbury, S. H. *J. Am. Chem. Soc.* **2009**, *131*, 7735–7741.

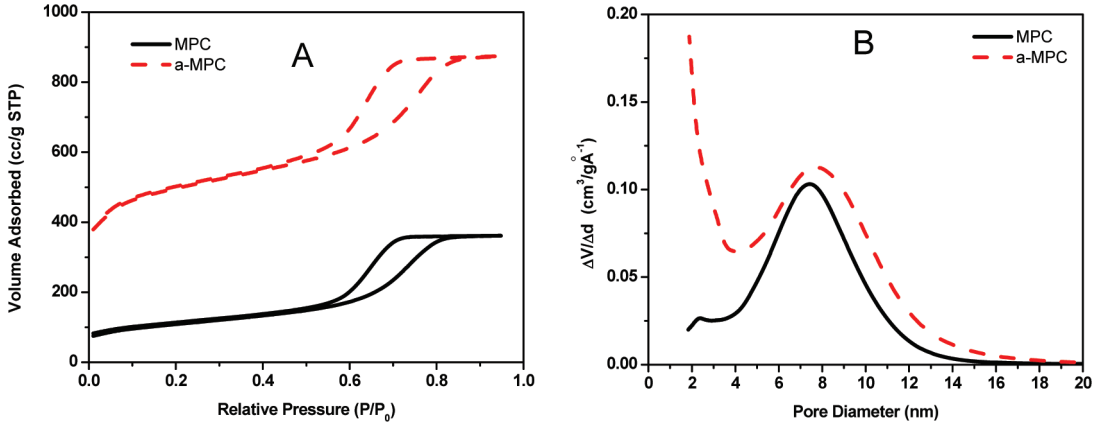

Figure 1. N_2 adsorption/desorption characterization of mesoporous carbon and KOH activated mesoporous carbon: (A) isotherms at 77 K; (B) pore size distribution calculated by BJH method by using the adsorption branch of isotherm.

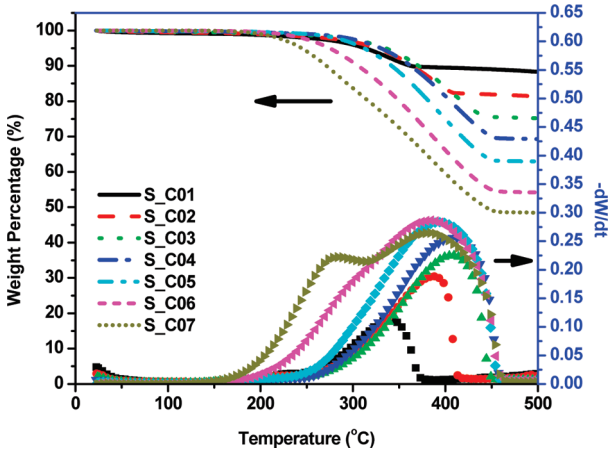

Figure 2. Thermogravimetric analysis (TGA) of S/C composites in nitrogen with heating rate of 10 °C/min. Lines represent the weight percentage (%) versus temperature; symbols represent the derivative weight loss versus time (dw/dt).

impregnation/drying procedure to attain samples with various loading by using a 10 wt % sulfur solution in CS_2. The solvent carbon disulfide was evaporated in a well-vented hood. After each impregnation/drying cycle, each sample was annealed at 140 °C for 1 h with protection of nitrogen gas. The annealing step stripped away the residual CS_2. The resulting samples are denoted as S_C01 to S_C07 with increasing sulfur loading of 11.7, 18.7, 24.8, 30.7, 37.1, 45.8, and 51.5 wt % determined by thermogravimetric analysis (TGA) in nitrogen. Shown in Figure 2 are the TGA curves and derivative weight loss versus time (dw/dt) of the S/C composites. The derivative weight loss versus time plots indicate the relative evaporation rate of sulfur from the S/C composites. At a fixed heating ramp of 10 °C/min, the evaporation rate of the sulfur from the S/C composites can be used as indirect evidence to locate the sulfur loaded on the bimodal porous carbon. Generally, the sulfur located in the micropores evaporates slower than that in the mesopores because of the strong adsorption of the micropores. However, because of the polymerizing nature of sulfur at temperatures above 170 °C,[1] the evaporation rate also depends on the weight percentage of sulfur on carbon. Nevertheless, the shoulder peak of the sulfur evaporation rate for sample S_C07 in Figure 2 suggests that a portion of the sulfur is located in the mesopores when the sulfur loading exceeds a certain weight percentage. The surface area and pore volume measurements discussed in the next section give more direct evidence of the correlation of the loading and the location of the sulfur on the bimodal porous carbon.

3.2.2. Surface Area and Pore Sizes. The surface area (SA) and pore size distribution (PSD) of the S/C composites were analyzed through N_2 adsorption/desorption measurements at 77 K and plotted in panels A and B in Figure 3 . The N_2 isotherms of these samples have a capillary condensation step centered at a relative pressure (P/P_0) of 0.7 and a H1 type hysteresis. The samples S_C01 to S_C05 have a bimodal pore size distribution with mesopores averaged at 7.3 nm. The cumulative pore volume of samples (Figure 3 C) with a sulfur loading less than 37.1 wt % shows an upward inflection point at a pore diameter of 3 nm; this is an indication that a portion of the pore volume and surface area of samples with a sulfur loading less than 37.1 wt % are attributed to small mesopores (pore size < 3 nm) and micropores. Figure 3 D illustrates the dependence of pore volume and surface area on sulfur loading. The micropore volume is completely filled up when the sulfur loading is above 37.1 wt %. The isotherm, surface area, and pore size distribution of the sample S_C05 (37.1 wt %) is close to those of the original mesoporous carbon (MPC) before activation. The sulfur loading of 37.1 wt % is most likely the critical point for these S/C composites: the micropores and small mesopores (< 3 nm) in the a-MPC can accommodate up to 37.1 wt % of elemental sulfur, higher sulfur loading could lead to the occupation of large mesopores. For example, the sample S_C07, at a high loading of 51.5 wt % of sulfur on the bimodal porous carbon, has a surface area of 146.9 m^2/g and a pore volume of 0.3 cm^3/g. Compared to the S/C composites made from carbons with only mesopores[2] or mainly micropores,[21] the S/C composites made from the bimodal meso/microporous carbon have prominent advantages of high surface area and large pore volume, which favor the adsorption of

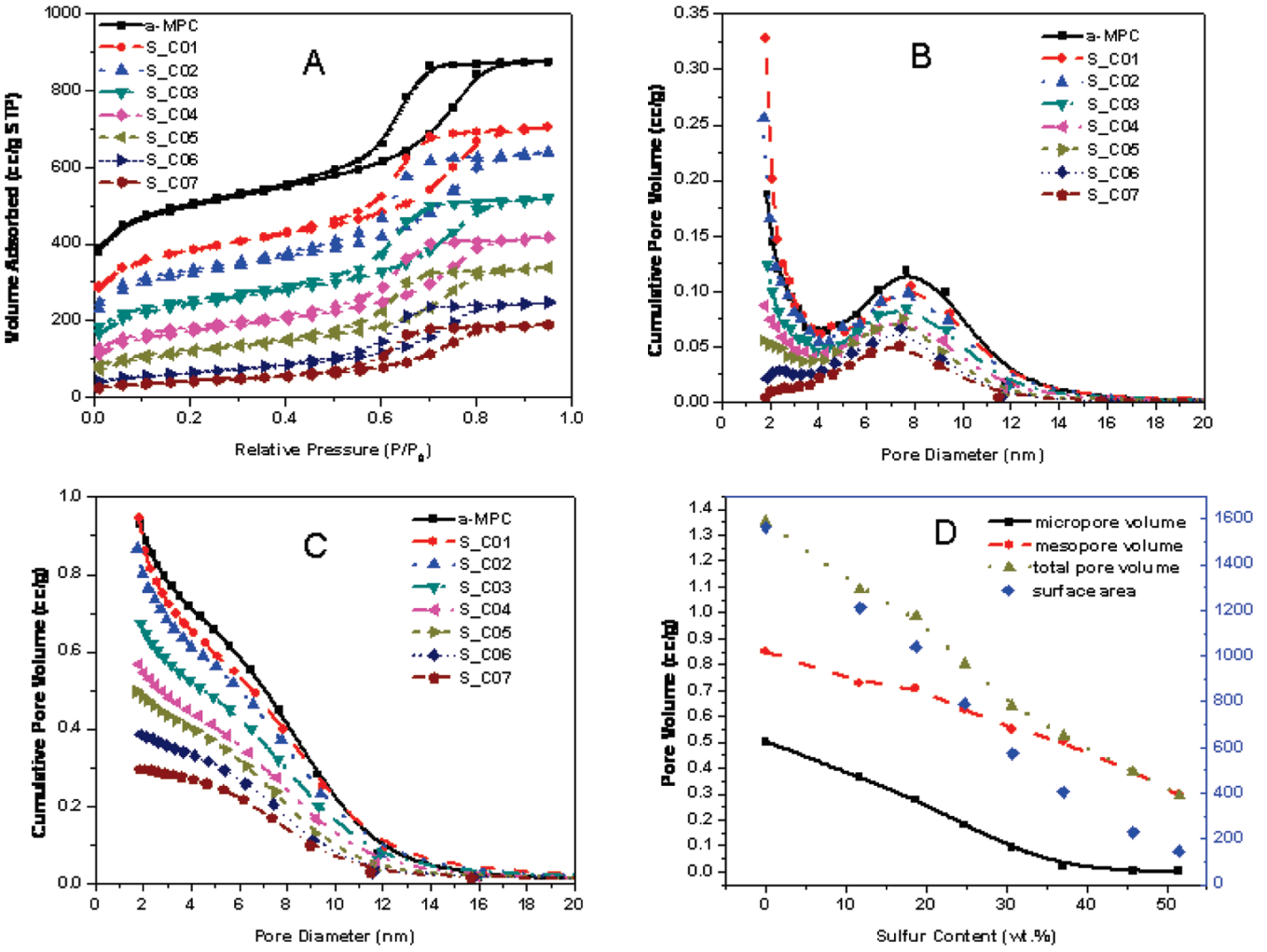

Figure 3. N_2 adsorption/desorption characterization of S/C composites with various sulfur loadings: (A) isotherms at 77 K; (B) pore size distribution calculated by BJH method using the adsorption branch of isotherm; (C) cumulative pore volume; and (D) pore volume and surface area versus sulfur loading. The sample a-MPC is the blank activated mesoporous carbon without S. The sulfur loading for samples S_C01 to S_C07 are 11.7, 18.7, 24.8, 30.7, 37.1 45.8, and 51.5 wt. %, respectively.

polysulfides and the mass transport of Li^+ during the battery operation.

3.2.3. High-Resolution Scanning Electron Microscopy (HRSEM) Characterization. In order to further confirm the porous structure of the S/C composites, the bimodal porous carbon and S/C composites have been compared through HRSEM images. Shown in Figure 4 are the HRSEM images of the pristine bimodal porous carbon and the sample S_C02. The images confirm the porous nature of bimodal carbon before and after sulfur loading. These two images show undistinguishable difference in morphology because that the sulfur resides inside the micropores (pore size less than 2 nm), which are not able to be observed by the HRSEM images. Therefore, the comparison of the HRSEM images of the bimodal porous carbon before and after sulfur loading is the direct evidence that the sulfur is loaded inside the micropores as we expected. This HRSEM observation coincides with the TGA and N_2 sorption measurements. Shown in panels C and D in Figure 4 are the elemental maps of carbon and sulfur for the S/C composite. These elemental maps confirm the sulfur is homogeneously distributed on the porous carbon. Because of the evaporation of sulfur under high vacuum and high-energy electron beam, the actual sulfur content of the sample during the imaging of the S/C composites varies with the exposure time of the sample to the electron beam in vacuum. A direct morphologic comparison of the S/C composites as a function of sulfur loading is difficult.

3.3. Battery Cycling. The electrochemical performance of the S/C composites with various sulfur loadings were tested by using 1.0 m bis(trifluoromethane)sulfonimide lithium (LiTFSI) in a mixed solvent of 1,3-dioxolane (DOL) and dimethoxyethane (DME) (volume ratio of 55:40). This electrolyte composition is reported to be an excellent electrolyte for lithium−sulfur rechargeable batteries because of the facts: (1) high solubility of lithium sulfide in the mixed solvent of DOL and DME, (2) good compatibility of organic components with the electrode materials, and (3) high ionic conductivity.[6,30,31]

(30) Rauh, R. D.; Abraham, K. M.; Pearson, G. F.; Surprenant, J. K.; Brummer, S. B. *J. Electrochem. Soc.* **1979**, *126*, 523–527.
(31) Peled, E.; Sternberg, Y.; Gorenshtein, A.; Lavi, Y. *J. Electrochem. Soc.* **1989**, *136*, 1621–1625.

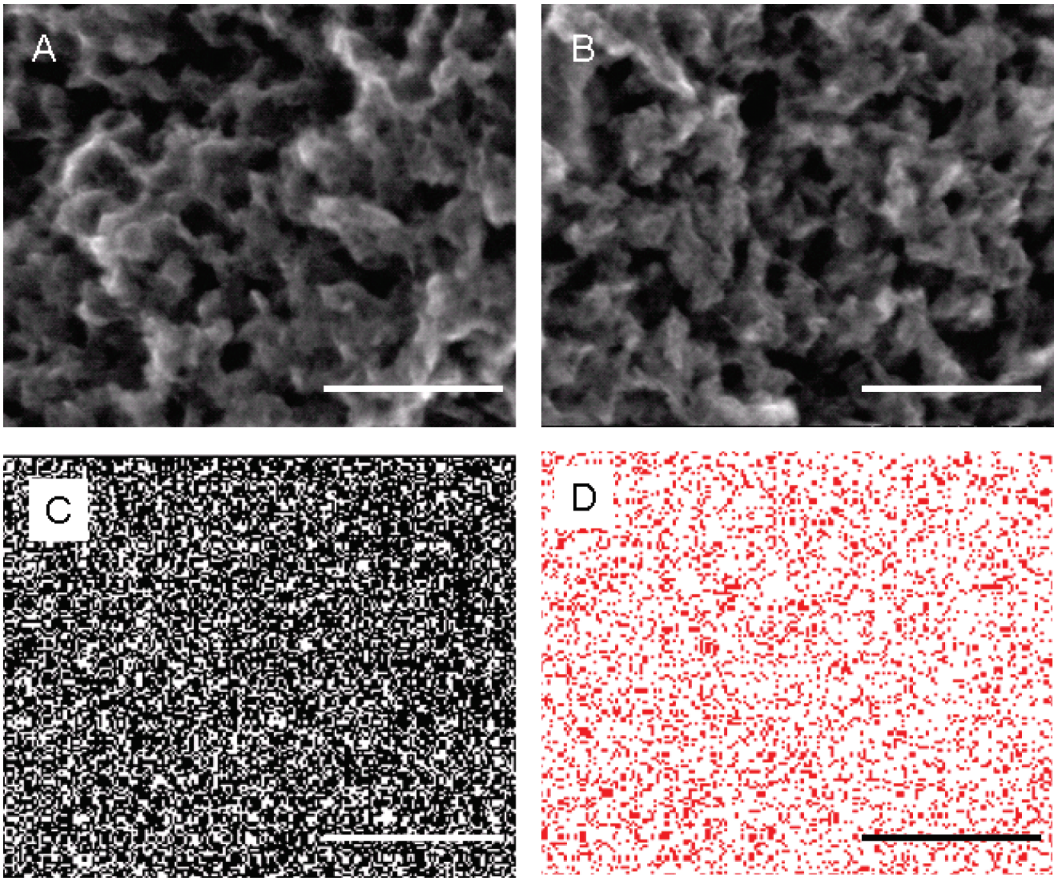

Figure 4. HRSEM images of (A) the bimodal porous carbon and (B) the S/C composite with 18.7% sulfur loading. Elemental maps of (C) carbon and (D) sulfur of the S/C composite. Scale bars represent 50 nm.

To illustrate the advantageous properties of the S/C composites prepared from the a-MPC, we prepared two additional S/C composite cathodes: one using the original MPC containing only mesopores, and a second using WVA-1500, an activated microporous carbon that contains mainly micropores. The surface area of WVA-1500 is 1760 m^2/g, which is comparable to that of the a-MPC. The specific capacities of these cathodes are plotted versus cycle numbers in Figure 5. The S/C composites prepared from mesoporous carbons including a-MPC and MPC had high initial discharge capacities. The initial discharge capacity decreased with the increase in sulfur loading: when the sulfur loading was 11.7 wt %, demonstrated by sample S_C01, the specific capacity of the initial discharge was as high as 1584.56 mA h g^{-1}, which was about 94.6% of sulfur utilization based on the theoretical maximum 1675 mA h g^{-1}; when the sulfur loading was 51.5 wt %, i.e., sample S_C07, the initial discharge capacity was 818.22 mA h g^{-1}. It is worth noting that the MPC supported S/C composite with 24.1 wt % sulfur had an initial discharge capacity of 1135.87 mA h g^{-1}. Of striking contrast, the S/C composite prepared from WVA-1500 with 25.2 wt % sulfur loading displayed a very low initial discharge capacity of only 387.64 mA h g^{-1}. Therefore, the presence of mesopores accounts for the high initial discharge capacity. Although the MPC supported S/C composite had a high initial discharge capacity, it had a very fast decay

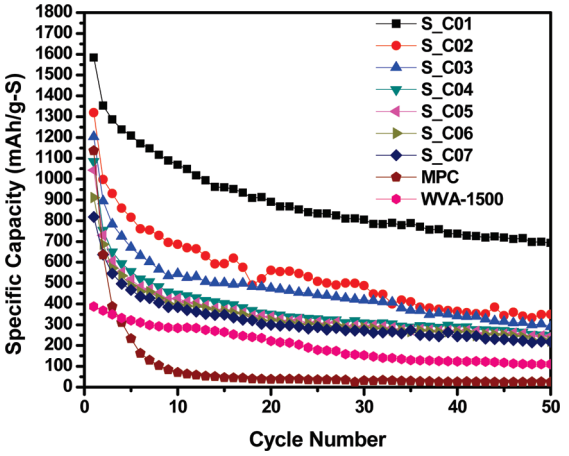

Figure 5. Specific discharge capacity of S/C composites that cycled in 1.0 m LiTFSI in DOL/DME (55:40) at 25 °C. The calculation of specific discharge capacities is based on the mass of sulfur.

of capacity in the following cycles. The capacity of the MPC supported S/C composite dropped to 163 mA h g^{-1} at the sixth cycle. The a-MPC and WVA-1500 supported S/C composites showed high retention of capacities in the cell cycling. The sample S_C01 retained a capacity of 804.94 $mAhg^{-1}$ after 30 cycles; and the WVA-1500 supported S/C composites had a capacity of 153.5 $mAhg^{-1}$ after 30 cycles; however, its initial discharge capacity was only 387.64 $mAhg^{-1}$. The comparison of the cycling performances of S/C composites supported by

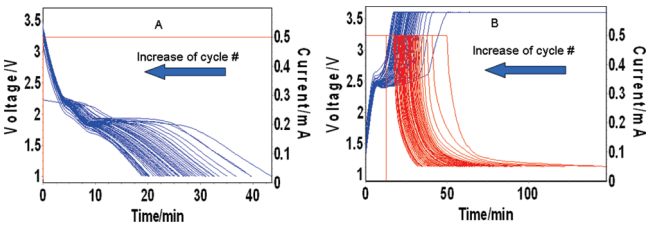

Figure 6. Cycling current (I) and voltage (V) curves of a Li/S battery composed of a cathode made from S_C03 S/C composite, an anode of Li foil, and an electrolyte of 1.0 m LiTFSI in DOL/DME (55:40). (A) Discharging cycles and (B) charging cycles. The battery was cycled between 1.0 and 3.6 V at 25 °C for 50 cycles. Current in red; voltage in blue.

MPC, WVA-1500, and a-MPC demonstrates the following points: (1) the mesopores enable the S/C composite to have a high initial discharge capacity; and (2) the micropores impart the retaining of cell capacity in the cycling. The a-MPC possesses both mesopores and micropores. The combination of meso/micropores of a-MPC makes it an excellent electrode material for Li/S batteries.

As mentioned earlier, the capacity decay of the Li/S battery is caused by the intrinsic polysulfide shuttle. As long as the concentration gradient of polysulfide exists in the Li/S battery, the polysulfide shuttle phenomenon cannot be eradicated. The physical adsorption of microporous materials such as a-MPC and WVA-1500 could mitigate the migration of sulfur; nonetheless, the sulfur transport from the cathode to anode is evidenced by the obvious capacity decay shown in Figure 5 and the cycling current (I) and voltage (V) curves shown in panels A and B in Figure 6. The cycling current (I) and voltage (V) curves in panels A and B in Figure 6 are plots of sample S_C03 cycling for 50 cycles with an electrolyte of 1.0 m LiTFSI in DOL/DME (55:40). The cell had two discharge voltage plateaus at 2.2 and 1.9 V, respectively, for the initial discharge. The first plateau is the discharge of sulfur and polysulfides (Li_2S_n, n stands for the number of sulfur atoms of the polysulfide anion) with $n \geq 6$, and the second plateau is the discharge of Li_2S_n with $n < 6$. These two plateaus progressively decreased in voltage and duration as the cycles were continued. The two plateaus diminished to 1.9 and 1.6 V after 50 cycles (Figure 6A). A typical charging $I-V$ curve of the Li/S battery has a curvy region at an average voltage of 2.4 V. The region has a slow increase of voltage during the charging because of the oxidation of polysulfide anions. A rapid increase in voltage follows the curvy region at the end of charging because of the depletion of polysulfide anions. The average voltage and the duration of the curvy region reflect the internal resistance and the charging capacity of the Li/S battery. The plot in Figure 6B shows that the average voltage of each cycle increases and the duration diminishes when the cycle number increases. Apparently, the cell capacity of the S_C03 cathode decreases and the cell resistance increases with the advancing of cycle numbers. All these changes are attributed to the polysulfide shuttle, which causes the irreversible migration of sulfur from the cathode to the anode.

4. Conclusions

The activation of mesoporous carbon created from a soft-template synthesis imparts high surface area to a carbon material with two sets of porosities. This bimodal porous carbon material is a suitable substrate for the S/C composite cathode material that possesses advantageous properties of high-energy and high-power over the cathodes made of mesoporous carbon or microporous carbon. The initial discharge capacity of the cells can be as high as 1584 mA h g^{-1} at a high current density of 2.5 A/g, which is better than the literature reported 1155 mA h g^{-1} at a much lower current density of 0.04 A/g.[18] The excellent performance of the bimodal porous carbon-supported S/C composite cathode is likely attributed to the synergetic effect of the hierarchically structured meso/microporosity: The microporosity gives high surface area and the micropore volume functions as a container that retains the sulfur species at the cathode region; the mesoporosity provides an avenue for the mass transport of Li ions and thus confers a high ionic conductivity to the cathode. Therefore, the cells can be discharged and charged at a high current density without compromising the cell capacity.

Acknowledgment. The authors thank the Oak Ridge National Laboratory for the financial support through a laboratory-directed research and development Grant S08-027. The synthesis and structural characterization of the bimodal porous materials and the S/C composites were conducted at the Center for Nanophase Materials Sciences, which is sponsored at Oak Ridge National Laboratory by the Scientific User Facilities Division, Office of Basic Energy Sciences, U.S. Department of Energy. C.D.L. thanks M. D. Pawel for proofreading the manuscript.